HYDROELASTIC TAILORING AND OPTIMIZATION OF A COMPOSITE MARINE PROPELLER

José P. Blasques, Christian Berggreen and Poul Andersen

Department of Mechanical Engineering, Technical University of Denmark
Nils Koppels Allé, Building 403, DK-2800 Kgs. Lyngby, Denmark
jpb@mek.dtu.dk

ABSTRACT

The following paper deals with the design and optimization of a flexible composite marine propeller. The blade shape is obtained from an existing high skew metal propeller. The aim is to tailor the laminate to control the elastic couplings and therefore the deformed shape of the blade. The development of a hydroelastic code is described first where the finite element method and boundary element method are used for the structural and hydrodynamic sub-models, respectively. The equilibrium between the elastic and hydrodynamic forces is obtained by direct substitution. NOMADm, a mesh adaptive direct search filter algorithm, is used together with DACE, a surface fitting algorithm, to determine the optimal laminate lay-up and blade pitch angle. The optimal configurations which reduce the fuel consumption for the combination of two load cases are found. The strength requirements are then analyzed using the Tsai-Wu failure criteria. The results show that it is possible to design a flexible composite marine propeller that will enable a reduction of the fuel consumption while withstanding the imposed loads.

1. INTRODUCTION

Anisotropic composite materials present different levels of elastic couplings which depend on the laminate lay-up. Among these, bending- and extension-twist couplings have been identified as a possible mean for the passive control of composite structures [1-,2-]. The aim here is to investigate the possibility of tailoring these elastic couplings to control the performance of a flexible composite marine propeller. The shape of the propeller blade will morph under load thus passively adjusting itself to the pressure loads of the different operational conditions. The optimal composite propeller is the one which most reduces the fuel consumption.

The use of elastic couplings to control the passive properties of different structures like aircraft wings, helicopter rotor blades and wind turbine blades has been extensively reported. The literature concerning the application of composite materials in the design of marine propellers is however limited. Lee et al. [3-] has optimized the laminate lay-up of a fixed pitch 0.305 m diameter composite marine propeller using genetic algorithms. The final design is shown to reduce the torque at one of the load conditions. An evaluation of the strength properties of a composite propeller blade with 1.4 m diameter has been presented by Lin et al. [4-]. The strength is analysed using the Hashin failure criterion and the results show the influence of the laminate type on the stress field. Marsh [5-] has presented an overview of the developments in the composite propeller industry. A few companies have realized the potential and claim to have designed composite marine propellers with passive properties. Nonetheless, no details of this work have yet been published.

The work described in this paper tries to extend the knowledge available in the field of design and optimization of composite marine propellers, and especially with the focus on larger marine propellers for merchant or naval vessels. The propeller blade considered throughout this paper is approximately four times larger than those described earlier in literature. The result will hopefully shed some light on the

possibility and potential of using composite propeller blades in large merchant or naval vessels. The hydrodynamic model is based on the boundary element method instead of the lifting line method applied in earlier papers. Moreover, the optimization of the fibre orientations is combined with the strength analysis in one design process. The two analyses have earlier been treated separately.

2. BLADE GEOMETRY AND MATERIAL PROPERTIES

The original propeller blade is part of a controllable pitch propeller installed on a military vessel. The propeller has 4 blades, a diameter of 4.4 meter and an expanded area ratio of 0.56. Its main geometrical properties are presented in Table 1.

r/R	θ_{skew} [o]	Rake/R	P/D	c/D	t/c	f/c
0.300	0.000	0.0000	0.90665	0.200	0.195	0.000
0.350	-6.033	0.0006	1.02277	0.230	0.159	0.032
0.400	-10.156	-0.0018	1.13893	0.260	0.131	0.040
0.500	-16.663	-0.0250	1.30864	0.320	0.091	0.036
0.600	-16.663	-0.0309	1.42662	0.360	0.067	0.027
0.700	-6.033	-0.0787	1.46216	0.385	0.050	0.020
0.800	6.542	-0.0910	1.38514	0.380	0.037	0.015
0.900	20.141	-0.0807	1.1867	0.320	0.029	0.009
1.000	36.932	-0.0299	0.8685	0.050	0.086	0.000

Table 1 - Geometrical properties of the propeller blade.

These types of ships typically operate at two speed conditions – cruising and maximum speed – which correspond to very distinct operational conditions (Table 2). The non-dimensional thrust and torque coefficients K_T and K_Q are defined as

$$K_T = \frac{T}{\rho n^2 D^4}, K_Q = \frac{Q}{\rho n^2 D^5} \quad (1)$$

where T, Q, ρ, n and D are the thrust, torque, water density, rotational speed and propeller diameter, respectively.

	No. Eng.	Power	n	V_s	J	P/D_{07}	K_T	K_Q	η_0	FC
	-	[kW]	[r.p.s.]	[m/s]	[-]	[-]	[-]	[-]	[-]	[Kg/h]
Cruising Speed	1	1410	1.8	7	0.742	0.925	0.056	0.0091	0.59	26.83
Maximum Speed	3	8380	2.33	11	0.901	1.465	0.176	0.0363	0.65	662.1

Table 2 – Data for the cruising and maximum speed operation conditions.

The composite marine propeller was designed using carbon/epoxy uni-directional reinforcements. The mechanical properties are presented in Table 3.

3. METHODOLOGY

The initial step of the analysis of the composite propeller consisted of the development of the structural and hydrodynamic sub-models. These models were then combined in the hydroelastic model which, for a steady incoming flow, determines the equilibrium between the structural and hydrodynamic forces. Once the hydroelastic model is set up it is possible to analyze the influence of the laminate lay-up on the propeller performance. An optimization model was then used to determine the laminate lay-up which will improve the propeller performance. The strength of the most optimal configurations was then studied using the Tsai-Wu strength index.

	Symbol	Units	Std CF
Young's Modulus	E_1	GPa	**UD**
Stiffness Modulus	E_1	GPa	135
	E_2	GPa	15
	E_3	GPa	15
Shear Modulus	G_{12}	GPa	5
	G_{13}	GPa	5.3
	G_{23}	GPa	2.9
Poisson's Ratio	ν_{12}	-	0.3
	ν_{13}	-	0.02
	ν_{23}	-	0.02
Ult. Tensile Strength	$\sigma_{1,t}^f$	MPa	1500
	$\sigma_{2,t}^f$	MPa	50
	$\sigma_{3,t}^f$	MPa	50
Ult. Comp. Strength	$\sigma_{1,c}^f$	MPa	1200
	$\sigma_{2,c}^f$	MPa	250
	$\sigma_{3,c}^f$	MPa	70
Ult. Shear Strength	σ_{12}^f	MPa	70
	σ_{13}^f	MPa	64
	σ_{23}^f	MPa	64
Density	ρ	kg/m^2	0.211
Thickness	t	mm	0.3

Table 3 – Mechanical properties of Carbon/Epoxy uni-directional reinforcement [6-].

3.1. Hydroelastic model

The displacement field is determined using the finite element method in the structural sub-model, and the hydrodynamic pressure field is likewise determined using the boundary element method in the hydrodynamic sub-model. The equilibrium between the hydrodynamic and structural parts is presented below. Thus, the combined analysis consists of determining the displacement vector {d} which satisfies [K]{d}={f}. Since {f} is a function of {d} the problem is nonlinear. Furthermore, {f} is only dependent of the state {d} which makes the problem suited for iterative solution. The direct substitution method has been chosen and its implementation is described next.

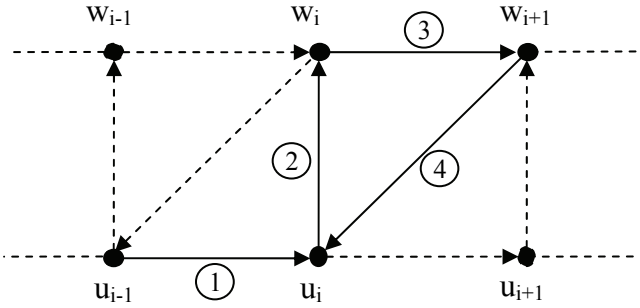

Figure 1 - Algorithm for the computation of the hydroelastic steady state.

In Figure 1 the subscript *i* indicates the iteration number, *u* is the displacements field determined by the structural model and *w* is the pressure field given by the hydrodynamic model. Each of the numbered steps is described below:

1) The displacement field is determined by the structural model for a given pressure distribution. At the first iteration the pressure distribution is taken from the original blade;
2) The hydrodynamic model mesh is updated based on the displacement field determined in 1).

3) A new pressure field is determined by the hydrodynamic model based on the new mesh.
4) The new pressure field given in the hydrodynamic model mesh is mapped into the structural model.

The process is repeated until convergence is achieved, i.e., equilibrium is found. The thrust and torque are calculated at each iteration and the method converges when the relative difference between iterations of the thrust and torque is less than 1%. It can be shown that the method is stable (see [7-]) and thus suited for the problem at hand. The displacement and pressure fields have been mapped based on the closest point and by linear interpolation, respectively.

3.1.1. Structural sub-model

The structural sub-model was developed in the commercial finite element package ANSYS (version 11) and used to determine the displacement field as a result of a given pressure distribution. In the first approach, the blade geometry was approximated by the mid-thickness lines of each section. A surface was subsequently defined and meshed with 8 node parabolic layered shell elements (SHELL99). The shape of the blade was obtained by setting the thickness of the elements at each node equal to that of the blade at the corresponding position. Since it was not possible to validate the results against experimental data, a second finite element model was developed following a different approach. The shape of the blade was defined by its volume and meshed using 20 node parabolic layered solid elements (SOLID191). A mesh convergence test on the displacements and stresses was conducted for each of the models.

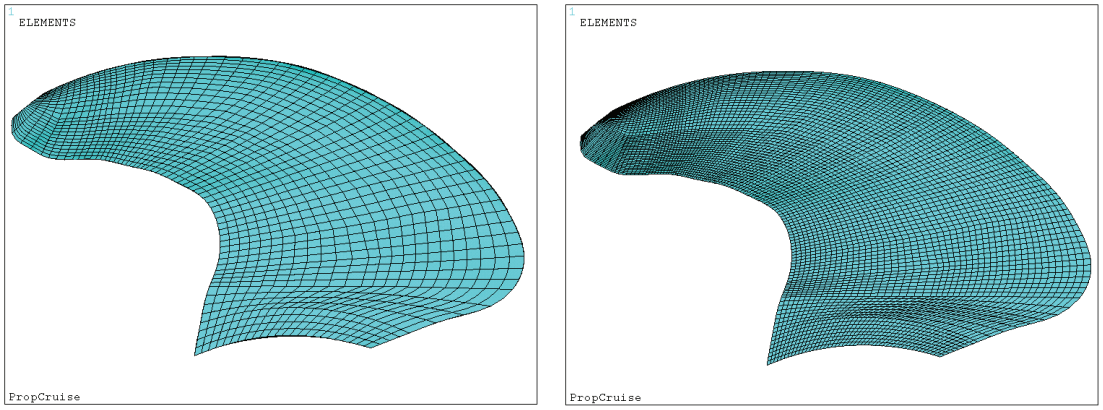

Figure 2 – (a) Mesh used for displacement analysis (left). (b) Mesh used for stress analysis (right).

The two models were compared in terms of their ability to predict the influence of the laminate lay-up on the thrust and torque forces (see [7-]). The results were found to be in good agreement. As shall be seen later, the displacements are the only necessary result from the structural model used in the optimization model. Hence, the first model using shell elements was chosen because it was less computationally expensive. When comparing the stress fields, there were some discrepancies between the predicted magnitudes of the stress. Generally, the stress field calculated by the second model should be more accurate than the shell model assuming mesh convergence for the stresses has been attained. However, for practical reasons concerning the element-wise orientation of the laminates, the shell model was used.

A total of 1440 and 5760 elements are required for the analyses of the displacement and stress fields, respectively (Figure 2). The model is constrained at the blade root to simulate the attachment to the blade hub. The centrifugal forces are applied as accelerations depending on the rotational speed. The number of layers is assumed constant and fixed at 32 throughout the blade and all layers are assumed to have the same thickness. The total thickness of the laminate is equal to that of its metal counterpart blade at the corresponding position. The layer angles may be defined element-wise.

3.1.2. Hydrodynamic sub-model

The hydrodynamic sub-model was used to determine the pressure field for a given blade shape. The inflow to the propeller is assumed to be uniform and steady, and viscous forces have not been accounted for. A total of 480 section points define the 450 elements which are arranged in a 15×15 three dimensional structured mesh (Figure 3) laid over the surface of the blade. The pressure is determined at 450 nodes placed at the center of each element whose corners are defined by the section points (which define the section lines). The pressure is integrated over the hydrodynamic mesh to determine the values of thrust and torque.

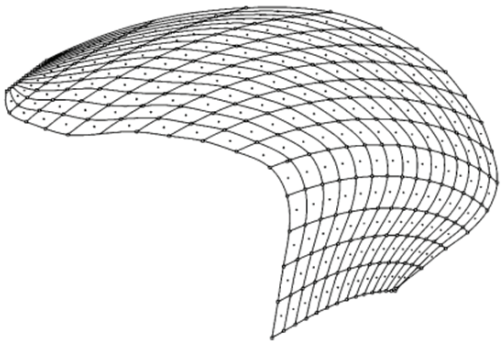

Figure 3 - Mesh of hydrodynamic sub-model (pressure side).

3.2. Optimization Model

In designing a marine propeller the speed at which the ship must sail is typically given and hence the thrust the propeller must generate. Thus, the optimal propeller will produce the desired thrust and minimize the torque, reduce the risk of cavitation, withstand the pressure forces and satisfy noise and vibration constraints. In this investigation the cavitation and vibration constraints have been neglected. The strength constraints have not been included in the optimization model, but have instead been studied separately. The optimization problem was therefore formally stated as:

$$\min_{\theta_n \in \mathbb{R}^n, \varphi_C \in \mathbb{R}\ ,\varphi_M \in \mathbb{R}} \quad \Delta t_C . SFOC_C . 2.\pi . n_C . Q_c(\theta, \varphi_C) + \Delta t_M . SFOC_M . 2.\pi . n_M . Q_M(\theta, \varphi_M) \qquad (2)$$

$$\begin{aligned} subject\ to: \quad & \frac{T_C^o(\theta, \varphi_C)}{T_C(\theta, \varphi_C)} - 1 \leq 0 \\ & \frac{T_M^o(\theta, \varphi_M)}{T_M(\theta, \varphi_M)} - 1 \leq 0 \\ & 0 \leq \theta_n < 180 \\ & \varphi_{C,min} \leq \varphi_C < \varphi_{C,max} \\ & \varphi_{M,min} \leq \varphi_M < \varphi_{M,max} \end{aligned}$$

where the subscript C, M and O indicate *cruising*, *maximum* and *original* (or required), respectively. The torque and thrust correspond to Q_C, Q_M, T_C and T_M, respectively. The design variables are the ply angles, θ, and the blade pitch angles φ_C and φ_M. Finally, Δt is the percentage of time the ship operates at each of the forward speed conditions, $SFOC$ is the specific fuel oil consumption and n is the propeller rotational speed.
Two operational conditions were considered, namely, cruising and maximum speed. The objective function is the combined fuel consumption. It was assumed that the ship operates 90% of the time at cruising speed and 10% at maximum speed, i.e., Δt_C=0.9 and Δt_M=0.1. The specific fuel consumptions for each of the operation conditions were estimated to be $SFOC_C$=0.190 Kg/KWh and $SFOC_M$=0.540 Kg/KWh. The design variables are assumed to vary continuously. Since the propeller is assumed to have controllable pitch, the pitch angles can be adjusted for each operational condition independently. The two thrust values are constrained from below, i.e., it is assumed that they may not be lower than the required thrust values. Note that inequality constraints were used instead of equality constraints on the thrust. This relaxation is possible due to fact that the thrust and torque are coupled in their variations. That is, an increase (or decrease) in the thrust will be accompanied by an increase (or decrease) in the torque.

3.2.1. Optimization algorithm
The optimization problem was solved using NOMADm; a derivative free, pattern-search algorithm [8-]. This algorithm is specially suited for the solution of nonlinear optimization problems where the gradients of the objective function – f – and constraints – C – are not available. The decision to opt for a gradient free method was motivated by the low accuracy of the presented hydroelastic model. With the lack of analytical sensitivities, the use of finite differences for the evaluation of the gradients was compromised by the low accuracy of f and C. The effect of the perturbations in the design variables was impossible to measure as these could not be distinguished from the variations due to the equilibrium iterations.
The NOMADm algorithm is essentially composed of a *search* and *poll* step. There are several different strategies for the search step. In this case, surrogate models of f and C have been used based on the DACE package. Thus, the initial step of the algorithm consisted on the evaluation of the computationally expensive functions f and C using a Latin hypercube sampling scheme. The aim is to generate a relatively large number of data sites that are "equally scattered" throughout the feasible region. A DACE model is subsequently fitted to the data to form an inexpensive surrogate. The MATLAB function *fmincon* is then used to generate a local minimizer of the surrogate where the functions f and C are consequently evaluated. Any new data site generated throughout is used to calibrate the surrogate. The poll step is invoked if the search step fails to find an improved point in the mesh. This step consists of evaluations of f and C in the mesh points around the incumbent solution.

3.3. Strength analysis
The strength of the blade is analyzed using the Tsai-Wu strength index (TWSI) as given in Equation (3). An index above one indicates material failure whereas an index below one indicates no failure has occurred.

$$TWSI = A + B \tag{3}$$

$$A = -\frac{\sigma_x^2}{\sigma_{x_t}^f \sigma_{x_c}^f} - \frac{\sigma_y^2}{\sigma_{y_t}^f \sigma_{y_c}^f} - \frac{\sigma_{xy}^2}{(\sigma_{xy}^f)^2} \frac{C_{xy}\sigma_x\sigma_y}{\sqrt{\sigma_{x_t}^f \sigma_{x_c}^f \sigma_{y_t}^f \sigma_{y_c}^f}}$$

$$B = \left(\frac{1}{\sigma_{x_t}^f} + \frac{1}{\sigma_{x_c}^f}\right)\sigma_x + \left(\frac{1}{\sigma_{y_t}^f} + \frac{1}{\sigma_{y_c}^f}\right)\sigma_y$$

4. RESULTS

Before proceeding with the optimization of the laminate lay-up several simple tests were conducted. The aim was to establish the influence of the fiber angle on the blade performance and strength. The study was conducted assuming the blade to be laminated with one single laminate using one single angle for all plies, i.e., $[\theta]_{32}$ over the entire blade. The ply reference axis is presented in Figure 4.

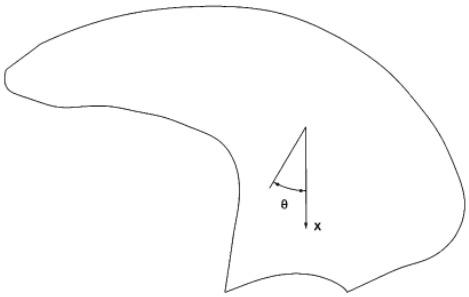

Figure 4 - Ply angle orientation reference axis

The angle was then rotated between 0° and 180° and the variation of the fuel consumption, thrust and torque were measured for both load cases (Figure 5). The results are shown as a ratio between the measured values and that of the original blade. The main changes in geometrical properties were measured in the radial distributions of pitch, camber and mid-chord positions. The pitch of the sections tends to be equal or lower than the original, while the camber tends to be larger in sections close to the hub and lower close to the tip. As expected, for both cases the blade has deformed in the up-stream direction. A ply angle, θ, in the range between 0° and 40° will result in a flexible tip and stiff lower part while a ply angle between 60° and 120° will reinforce the tip while making the lower part of the blade closer to hub more flexible.

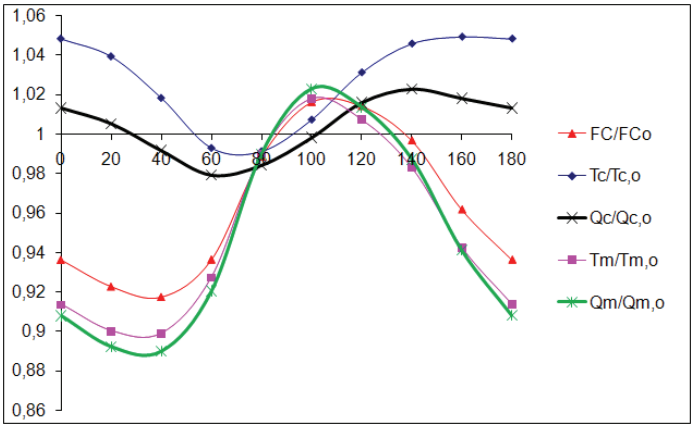

Figure 5 - Influence of the lamina angle on the thrust, torque and combined fuel consumption, assuming original pitch angles.

The curves in Figure 5 were affected by the blade pitch angle which can be used to compensate for the increase or decrease in the thrust forces. Note that these have to remain equal to those of the original propeller blade.
Regarding the strength requirements, the critical areas were identified as the trailing edge and hub areas. These areas were therefore locally reinforced (Figure 7 (b)) where area 1, 2, 3 and 4 were laminated using $[-45^o]_{32}$, $[0^o]_{32}$, $[0^o]_{32}$ and $[90^o]_{32}$. In the optimization model the angles in these areas is not varied but kept constant at the values specified.

4.1. Optimization of laminate lay-up

In the first approach it was assumed that the design variables were the orientation of the different layers through the thickness of the laminate. Thus, the following laminate configurations were tested: $[\theta_1]_{32}$, $[(\theta_1)_8, (\theta_2)_8, (\theta_3)_8, (\theta_4)_8]$ and $[(\theta_1)_8, (\theta_2)_8]_s$. All configurations converged to approximately the same results, i.e., to the laminate $[40^o]_{32}$. The resulting values of fuel consumption reduction and blade pitch angles are presented in Table 4. At maximum speed the thrust and torque are exactly equal to that of the original blade, however, at cruising speed a 4.2% reduction in the fuel consumption (corresponding to 1.12% in the combined case) was achieved.
These results indicate that the variation of the ply angles through the thickness has little influence on the blade response. Thus, the second approach consisted in defining the ply angles at each element as a function of its position in space. The approach is inspired by the results from Parnas et al. [9-] where cubic fiber paths and Bezier curves are used to optimize the fiber angles and thickness of a composite structure. The determination of the angle is as illustrated in Figure 6 (a). The ply angle at an element in position A is equal to the angle θ_e. This angle is determined by the tangent to a second degree polynomial defined by the points c_0, c_1 and c_3. The design variables in this case are the measures y_1 and y_2. The point c_0 and the coordinates z_1 and z_2 are kept fixed.

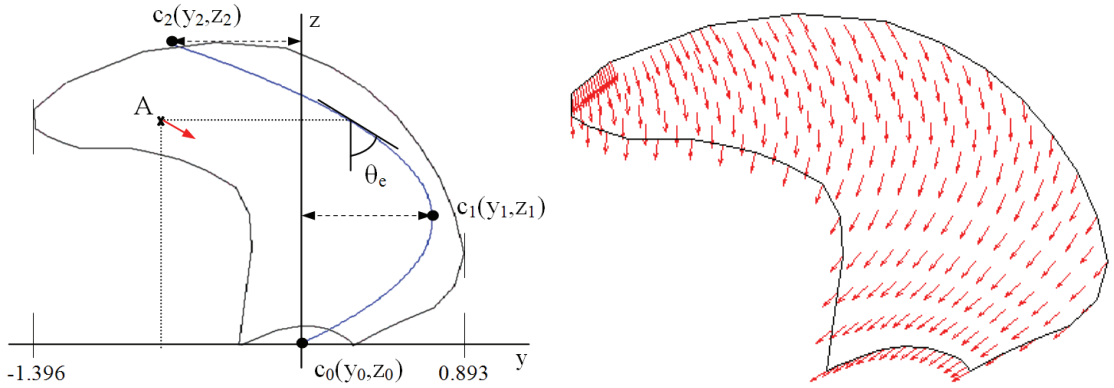

Figure 6 – (a) Definition of the second degree curved fiber path (left). (b) Resulting fiber angles obtained using curved fiber paths (right).

The following laminates were tested $[\theta_1(y_1,y_2)]_{32}$, $[(\theta_1(y_1^1,y_2^1))_{16}, (\theta_2(y_1^2,y_2^2))_{16}]$, $[(\theta_1(y_1^1,y_2^1))_8, (\theta_2(y_1^2,y_2^2))_8$, $(\theta_3(y_1^3,y_2^3))_8$, $(\theta_4(y_1^4,y_2^4))_8]$. As before the results were not sensitive to variations of the angles through the thickness. The most optimal laminate was $[\theta_1(0.756,0.677)]_{32}$. The resulting fiber angles are presented schematically in Figure 6 (b). This approach resulted in a further decrease of the fuel consumption as presented in Table 4.

It is interesting to note that the two design configurations presented above have the fact that they promote a flexible tip in common. In Figure 7 (a) the displacement sum for the curved fiber path configuration is plotted, and it is clear the effect of a flexible tip.

Laminate		Cruising Speed			Maximum Speed			Combined
		(P/D_{07})	$T_C/T_C^{Original}$	$\%FC_{saved}$	(P/D_{07})	$T_M/T_M^{Original}$	$\%FC_{saved}$	$\%FC_{saved}$
$[\theta_1]_{32}$	$[40^o]_{32}$	0.5438	1.00	4.2	2.412	1.00	0	1.12
$[\theta_1(y_1,y_2)]_{32}$	$[\theta_1(0.756,0.677)]_{32}$	0.5122	1.00	4.7	2.550	1.00	0	1.25

Table 4 - Results for the two optimal laminate configurations.

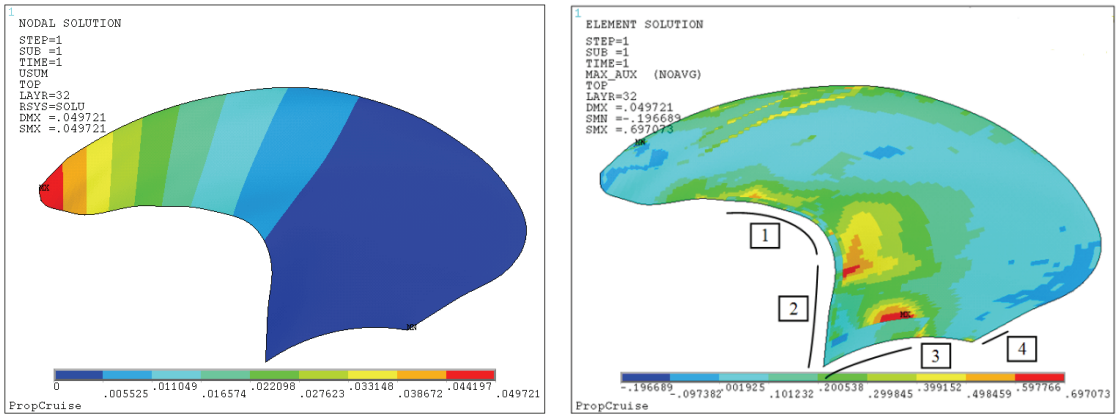

Figure 7 – (a) Displacement plot for the optimal composite blade with curved fiber paths (left). (b) Maximum TWSI over all layers for the optimal propeller blade with curved fiber path (right).

4.2. Strength analysis

The last step in the design process consisted of the analysis of the stress field in terms of the TWSI (Figure 7 (b)). The local reinforcements proved effective. The maximum TWSI measured for both laminate configurations was around 0.7 indicating that no failure has occurred. Although this value might correspond to an unacceptably low safety factor, it indicates that with finer tailoring of the laminates it is possible to build a flexible composite marine propeller blade which withstands the subjected loads.

5. CONCLUSIONS

A framework for the design and optimization of composite marine propellers has been presented. The laminate lay-up of a composite propeller blade with high skew was optimized for two different load conditions – cruising and maximum speed. Two different approaches have been explored, where the first assumes constant fibre angles throughout the blade and the second uses curved fibre paths. The optimal lay-ups have enabled a reduction of the combined fuel consumption around 1.2% corresponding to a decrease of 4.5% for the cruising condition and no reduction for the maximum speed condition. The largest variations in the blade shape were observed in the radial distributions of pitch, camber and mid-chord positions. The optimal configurations promoted a flexible tip and a stiff body close to the hub. The strength of the blade was analysed in terms of the Tsai-Wu strength index and the leading edge and hub regions were identified as the critical areas. The blade was therefore reinforced in these regions prior to the optimization procedure. It is shown that the maximum failure index is around 0.7 for both optimal configurations. The results indicate that it is possible to

build a flexible composite marine propeller which outperforms its original metal counterpart while resisting the imposed loads.

ACKNOWLEDGEMENTS

This work has been performed within the Network of Excellence on Marine Structures (MARSTRUCT) and has been partially funded by the European Union through the Growth Programme under contract TNE3-CT-2003-506141.
The invaluable support and advice given by Associate Professor Mathias Stolpe, Department of Mathematics, Technical University of Denmark, is gratefully acknowledged.

REFERENCES

1- Berring P., Branner K., Berggreen C., and Knudsen H. W., "Torsional Performance of Wind Turbine Blades – Part I: Experimental Investigation", *16th International Conference on Composite Materials (ICCM-16),* Kyoto, Japan, July 8-13, 2007
2- Branner K., Berring P., Berggreen C., and Knudsen H. W., "Torsional Performance of Wind Turbine Blades – Part II: Numerical Verification", *16th International Conference on Composite Materials (ICCM-16),* Kyoto, Japan, July 8-13, 2007
3- Lee Y.J. and Lin C.C., "Optimized design of composite propellers", *Mechanics of advanced materials and structures*, 2004;11:17-30.
4- Lin H.J., Lin J.J., Chuang, T.J., "Strength evaluation of a composite marine propeller blade", *Journal of Reinforced Plastics and Composites*, Vol.24, 2004;17:1791-1807.
5- Marsh G., "A new start for marine propellers?", *Reinforced Plastics*, December, 2004.
6- Peters S.T.,"Handbook of composites", *Chapman and Hall*, 2nd Edition, 1998.
7- Blasques J.P., "Composite materials marine propeller", Master thesis, Department of Mechanical Engineering, Technical University of Denmark, 2007.
8- Booker A.J., Dennis J.E., Frank P.D., Serafini D.B., Torczon V., Trosset M.W., "A rigorous framework for the optimization of expensive functions by surrogates", Technical Report CRPC-TR98739-S, Center for Research on Parallel Computation, Rice University, 1998.
9- Parnas L., Oral S. and Ceyhan Ü., "Optimum design of composite structures with curved fiber paths", *Composites Science and Technology*, 63, 2003, 1071-1082.